# New $\beta$-decay spectroscopy of the $^{137}$Te nucleus

M. Si (司敏) [1] R. Lozeva [1,2,*] H. Naïdja [3] A. Blanc,[4] J.-M. Daugas,[5,6] F. Didierjean,[2]
G. Duchêne [2] U. Köster,[4] T. Kurtukian-Nieto [7] F. Le Blanc [1,2] P. Mutti,[4]
M. Ramdhane [8] and W. Urban[9]

[1]*Université Paris-Saclay, IJCLab, CNRS/IN2P3, F-91405 Orsay, France*
[2]*Université de Strasbourg, IPHC, 23 Rue du Loess, F-67037 Strasbourg, France*
[3]*Université Constantine 1, LPMS, DZ-25000 Constantine, Algeria*
[4]*Institut Laue-Langevin, F-38000 Grenoble Cedex 9, France*
[5]*CEA/DAM Île-de-France, F-91297 Arpajon Cedex, France*
[6]*Université Paris-Saclay, CEA, CNRS, Inserm, SHFJ, BioMaps, F-91401 Orsay, France*
[7]*CENBG, CNRS/IN2P3, Université de Bordeaux, F-33170 Gradignan Cedex, France*
[8]*LPSC, CNRS/IN2P3, Université de Grenoble Alpes, F-38026 Grenoble, Cedex, France*
[9]*Faculty of Physics, University of Warsaw, PL-02093 Warsaw, Poland*

**Background:** Nuclear spectroscopy of neutron-rich isotopes provides important information on their nuclear structure and has a valuable impact on the modeling of the *r*-process path. Particularly interesting are nuclei close to doubly-magic species, e.g., $^{132}$Sn, with only several valence particles. Such is the barely explored $^{137}$I nucleus, investigated here in detail.

**Purpose:** To establish excited states in $^{137}$I, $\beta$ decay of the $^{137}$Te ground state is studied. In addition, the unknown $\beta$-delayed neutron-emission channel of $^{137}$Te to $^{136}$I is inspected. Search for levels and for candidates for Gamow-Teller and first-forbidden transitions between the mother nucleus and excited states in the daughter nucleus is conducted within the experimental observations.

**Methods:** $\beta$-delayed $\gamma$-ray spectroscopy is employed to study excited states in $^{137}$I. The nucleus is populated in the decay of a mass-separated beam of $^{137}$Te, produced in neutron-induced fission of $^{235}$U.

**Results:** The new level scheme of $^{137}$I populated in $\beta$ decay is established. The half-life $T_{1/2}$ of $^{137}$Te is determined to be 2.46(5) s. The $\beta$-delayed neutron-emission probability $P_n$ value of $^{137}$Te is deduced as a lower limit to be 2.63(85)%.

**Conclusions:** The experimental results are an important input to the theoretical description of nuclei in the region, being well interpreted within large-scale shell model calculations, and provide essential information on the first-forbidden transitions beyond $N = 82$ and $Z = 50$.

## I. INTRODUCTION AND MOTIVATION

Close to the double-shell closures in the nuclear chart, with a good example being the $^{132}_{50}$Sn$_{82}$ nucleus, the nuclear shell model remains a major structural framework to understand such magic species and their neighbors. By investigating the nuclear configuration of states around the $^{132}$Sn core, the extension of the magic core may be traced. Thus, the polarization effect of valence particles on this core can be studied in detail [1,2]. Valuable information on the nucleon-nucleon effective interaction and single-particle excitation energies is also obtained or inferred from experimental data. Furthermore, with increasing neutron number, a variety of new phenomena are predicted for these nuclei, e.g., the existence of neutron skin, vanishing of standard magic numbers, or opening of a new subshell gap [3–5]. These phenomena

challenge recent competitive studies and boost the quest for new data on more and more neutron-rich species. In our recent review on $^{136}$Te with two valence protons and two valence neutrons outside the doubly magic $^{132}$Sn core, we reported on observed deviations of transition rates from the ones predicted by the shell-model calculations [6]. On the other hand, for the iodine isotopic chain (with proton number $Z = 53$), we reviewed the $^{136}$Te $\beta$ decay to excited levels in $^{136}$I [7], and found that the newly established experimental levels compare very well with the shell-model theory. Therefore, it is of special interest in this work to continue our investigations for three-valence-proton systems beyond the magic number $Z = 50$ and gain such important information on the nuclear structure in the region. An isotone of $^{136}$Te, the current $^{137}$I nucleus (with neutron number $N = 84$) is a very interesting case since also its low-spin excitations are not explored in detail. Several intermediate-spin states in this nucleus, addressed in our review on $^{135–139}$I nuclei [8], show a similar tendency to the Te isotopic chain. Namely, three isotones have

rather similar trend of excitation energies and transition rates of first excited states with the increase of $N$, and slowed-down collectivity.

Although the excess of particles could polarize the $^{132}$Sn core and lead to collective behavior in $^{137}$I, detailed knowledge on the shell evolution of nuclei at such extreme proton-neutron ratios is still missing. The three valence protons in the iodines [7] are also regarded as a cluster [9] to explain some features of these nuclei [10]. It is a very interesting exploration field, though only the yrast states could be studied in both thermal neutron-induced $^{235}$U fission [11] and energetic neutron-induced $^{238}$U fission [8]. Many of the non-yrast states could not be populated by such a reaction. Based on the knowledge of the only previous $\beta$-decay work [12], the data on $A = 137$ are relatively scarce as compared to the $A = 135$ isotope. Only five excited states with excitation energy of up to 1169 keV and nine $\gamma$-ray transitions in $^{137}$I in the $\beta$ decay of $^{137}$Te are associated with the $^{137}$I decay scheme [13]. Therefore, new results on $^{137}$I are highly demanded. Interestingly, study of this decay was attempted four decades ago at LOHENGRIN [14,15], the main difference compared to today being a less efficient detection system then. Benefiting from new developments, more efficient systems, as well as a better experimental technology with radioactive neutron-rich beams, the majority of neutron-rich nuclei could be investigated by spectroscopy of the fission products directly. A product of such fission is $^{137}$Te and we report its $\beta$ decay in this work.

## II. EXPERIMENT

A $^{235}$U target is exposed to a neutron flux of $5 \times 10^{14}$/cm$^2$ s in an in-pile position of the high flux reactor of Institut Laue-Langevin (ILL). Fission fragments, produced by the thermal neutron-induced fission, recoiling from the target at kinetic energies of several tens of MeV are stripped to high charge states, $Q$, ranging typically from about $Q = 17$ to $Q = 26$. The LOHENGRIN recoil separator [16] separates these ions according to their mass to ionic-charge ratio $A/Q$ and their kinetic-energy to ionic-charge ratio $E/Q$. Unlike electromagnetic mass separators, e.g., ISOLDE, that separate singly-charged ions, an $A/Q$ selection at a recoil separator provides a not necessarily unique mass $A$ identification. For example, depending on the selected $Q$, a cocktail beam containing different $A$ at different $Q$ with a very similar $A/Q$ ratio could appear. Setting $A/Q = 137/23 = 5.96$ would lead to a simultaneous separation of $A'/Q' = 131/22 = 5.96$ and $A''/q'' = 143/24 = 5.96$, all reaching the focal plane within 1–2 mm lateral distance. This would not allow one to physically separate beams that are about 10 mm wide [17], and would thus render a unique assignment of observed $\gamma$ rays to a specific mass impossible. The $A/Q$ ratios 137/21 and 137/25 are more favorable because other masses have sufficiently different $A'/Q'$ ratios that they reach the focal plane at about 15 mm lateral distance, e.g., they are largely suppressed by the mass-defining diaphragms. As the mass resolving power of the LOHENGRIN spectrometer depends on the size of the target and of the mass-defining diaphragms, in the present experiment an 8 mm wide target was used to favor intensity
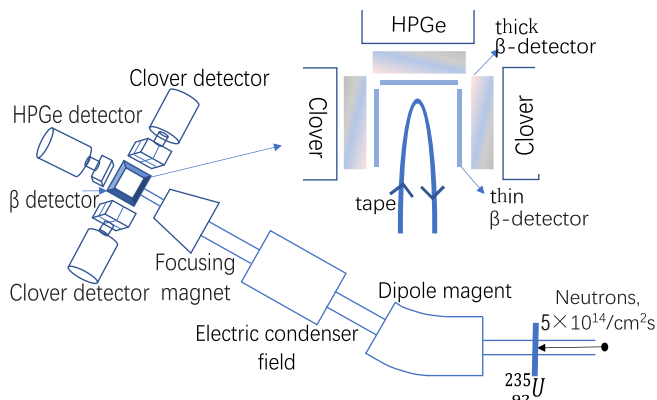


FIG. 1. The setup of this experiment.

over mass resolution. Therefore, still, the suppression is not perfect and a small fraction of ions belonging to the tails of neighboring $A'/Q'$ can reach the detection setup. Strong $\gamma$ rays belonging to the decay of $A'$ nuclides with high fission yield will be detected too; e.g., $^{142}$Cs is observed in the $A/Q = 137/25$ setting, while mass $A = 142$ isobars are absent for an $A/Q = 137/21$ setting. Hence, two separate runs are performed with two different $Q$ settings, where the respective neighboring masses $A'/Q'$ ratios have no disturbing mass $A'$ in common. Only $\gamma$ rays that are observed in both data sets with identical relative intensity ratios can be uniquely assigned to the chosen $A = 137$ of interest.

Using the technique described in Ref. [18], the mass-separated beams were transported to the focal plane behind a focusing magnet [19] as shown in Fig. 1. An experimental setup was built using the $\beta$-decay station of plastic detectors in $4\pi$ geometry from the LOENIE $\beta$-delayed neutron detector, arranged similarly to a box [20]. It consisted of a stack of thin and thick $\beta$-plastic detectors, arranged just in front of the Ge detectors. Each plastic was read out by two photomultipliers on each side, used in coincidence to deliver timing information. The detectors stacks are placed around a vacuum chamber that supported a movable tape, used to evacuate implanted long-lived radioactivity (see Fig. 1). The duty cycle was adapted to the half-life ($T_{1/2}$) of the isotope of interest.

The beam chopper was open for 3 s for the grow-in phase, then closed for 5 s, allowing 3 s for the decay measurement and 2 s for tape movement before the next measurement cycle. Emitted $\gamma$ rays were detected by two clover detectors ($4 \times 50 \times 80$ mm$^3$, not tapered, surrounded by bismuth germanate (BGO) anti-Compton shields, that were only used as passive shielding) and one standard 60% coaxial high-purity germanium (HPGe) detector in close geometry (see Fig. 1). The average energy resolution of the combined Ge detection array was 2.66(6) keV at 1.4 MeV.

The $\gamma$-ray detection efficiency of our detector system was calibrated with a 2 kBq $^{182}$Ta source and complemented with relative efficiencies derived from transitions in the $A = 136$ mass chain nuclides [7] (studied in a parallel experiment [21]) to cover intermediate and high energies up to 4.5 MeV. The energy range between and beyond known transitions was
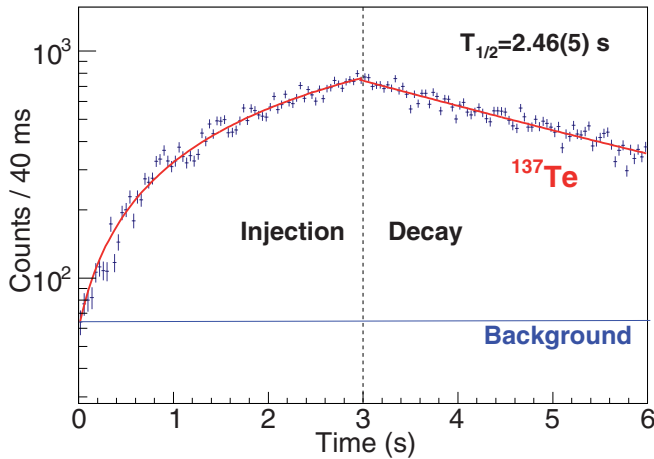
FIG. 2. Time distribution of $^{137}$Te $\beta$-decay events fitted with the resulting half-life.

complemented with simulated data. The absolute $\gamma$-ray efficiency was 0.69(3)% at 1 MeV. Data were collected by digital triggerless VME electronics and analyzed offline.

## III. DATA ANALYSIS AND RESULTS

### A. Half-life of $^{137}$Te

The $\gamma$-ray energy and the timing information with respect to the chopper cycle are used to construct the "chopper time-energy" matrix. This matrix allows monitoring the intensity of $\gamma$ rays within the measurement cycle. By gating on known $\gamma$ rays in $^{137}$I, we obtain the decay curve of $^{137}$Te. We summed up the time distributions of four known $\gamma$ rays in this decay (129, 243, 469, and 554 keV, each peak fitted by subtracting Compton background with gates right and left of the full energy peak). The half-life is obtained by fitting with a single exponential plus constant background using a chi-square minimization procedure (see Fig. 2). It results in $T_{1/2} = 2.46(5)$ s, reported in Table I, together with values from the literature. The quoted uncertainty combines statistical error and fit error.

We note that the fission yield of lower-$Z$ isobars, e.g., $^{137}$Sb, are much lower ($\ll 1\%$ with respect to $^{137}$Te [22]). Only a very weak hint of a $\gamma$ ray near the first excited and expectedly strongest transition in $^{137}$Te of 61.8 keV was observed in the $Q = 21$ data set (Fig. 3), but not in the $Q = 25$ data set. None of the other $\gamma$ rays belonging to the $^{137}$Sb decay to $^{137}$Te, as known from our RIKEN data [23], could be observed. This confirms that the relative fission yield of $^{137}$Sb is indeed negligible, and indirect (Bateman) contributions from $^{137}$Sb decay to $^{137}$Te can be safely ignored in our analysis of the grow-in and decay behavior.

TABLE I. $\beta$-decay half-life measured in this work compared with literature values.

| Nucleus | $T_{1/2}^{exp}$ (s) | $T_{1/2}^{lit}$ (s) |
|---------|---------------------|---------------------|
| $^{137}$Te | 2.46(5) | 2.49(5) [12], 2.1(1) [15], 2.08(40) [24] |

### B. $^{137}$Te $\beta$ decay to excited states in $^{137}$I

In the previous $\beta$-$\gamma$ spectroscopic study of $^{137}$I, five excited levels and nine $\gamma$ transitions were established [13], far below the $Q_\beta$ value of 7053(9) keV (see Sec. III D). In the present work, the $\beta$-delayed $\gamma$-ray spectrum of $^{137}$I is obtained by applying $\beta$-$\beta$ coincidence conditions to all Ge data. As we have thin and thick detectors, in order to improve efficiency we combine $\beta$ signals from these two types of detectors from the stack (see Fig. 1) within a time window of 100 ns, called here $\beta$-$\beta$ coincidence condition. This combination is regarded as a $\beta$ trigger (or $\beta$ gate) for the detection of $\gamma$ rays after $\beta$ decay. The $\beta$-gated $\gamma$-ray spectrum for different $A/Q$ settings on $Q = 21$ and $Q = 25$, as taken in our measurement, is shown in Fig. 3. One can clearly see, as marked by their energies, that in both settings the transitions from $^{137}$I are well identified. The main background comes from the $^{137}$Xe granddaughter nuclei, while for $Q = 25$ also $^{142}$Ba (with well known $\gamma$ rays) contributes to the background. In order to subtract the background from long-lived nuclei, the analysis is performed under the condition that the selected time window corresponds to the chopper decay part (3 s). The chopper off (last 2 s of the cycle) was subtracted from this decay (see Fig. 4). The long-lived activity could also be identified from the $T_{1/2}$ behavior of detected $\gamma$-rays. This subtraction is only qualitative to enhance the visibility of weak transitions, while quantitative data are determined from unsubtracted decay spectra. In this work we observed transitions known previously from $\beta$ decay of $^{137}$I [12] and fission [8,11] data.

With the aim to expand and establish a new level scheme of $^{137}$I from this new $\beta$ decay data, $\beta$-$\gamma$, $\gamma$-$\gamma$ (mutual) coincidences, and $\gamma$ intensity balances are used. The $\gamma$-$\gamma$ coincidence relations are constructed between the Clover detectors and the coaxial HPGe detector versus the Clover detectors.

For all these, we always used a $\beta$-gate with the detected $\gamma$-signal to suppress $\gamma$-ray background from the environment and from ions stopped in the mass-defining slit upstream. In Fig. 5, we show a spectrum gated on the 243.6 keV transition corresponding to the first excited state in $^{137}$I, where 15 cases of mutual coincidences could be found. Four of them are consistent with the previous knowledge: 129.5, 357.2, 469.7, and 925.9 keV. Six of them are used to construct six new excited levels: 609.6, 974.4, 1155.4, 1833.7, 2047, and 2170.2 keV. In Fig. 3, the 974.4 keV $\gamma$ peak sits on the tail of a background $\gamma$ in the $Q = 25$ (red) spectrum and is thus weak in the $Q = 21$ (blue) spectrum. As it has a very strong mutual coincidence with the 243.6 keV $\gamma$ ray, we propose to place this transition on top of the known 243.6 keV level. Due to weak statistics, for the 1833.7, 2047, and 2170.2 keV transitions we present, in addition, their gated spectra, illustrated in Fig. 5. The weakly seen 2047 keV $\gamma$ ray in Fig. 3, is marked as tentative. The new 227.1 keV transition, found in the 243.6 keV gated spectrum, shown in Fig. 5, is also in coincidence with the 229.1 keV line (in the 227 keV gated spectrum; see Fig. 6), and all transitions deexciting the level 373.1 keV such as the 129.5 keV line. As its energy, in addition, fits the energy difference between the 600.6 and 373.1 keV levels, we place it as a new transition in the level scheme (see Fig. 8 ). The
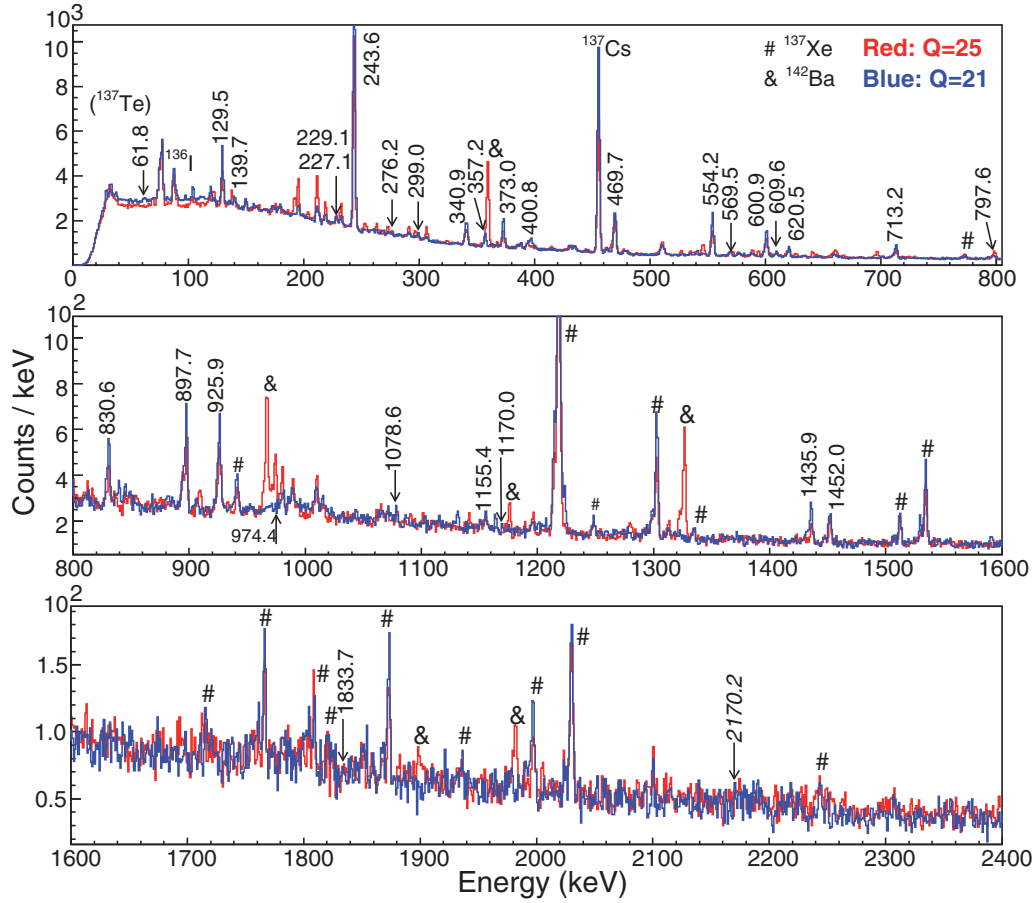
FIG. 3. The $\beta$-gated $\gamma$-ray singles spectrum obtained following the $\beta$ decay of $^{137}$Te for both $Q$ settings. Peaks belonging to $^{137}$I are marked by their energies. The main background comes from $^{137}$Xe granddaughter nuclei and a $^{142}$Ba contamination lines for $Q = 25$ coming from the decay of $^{142}$Cs.
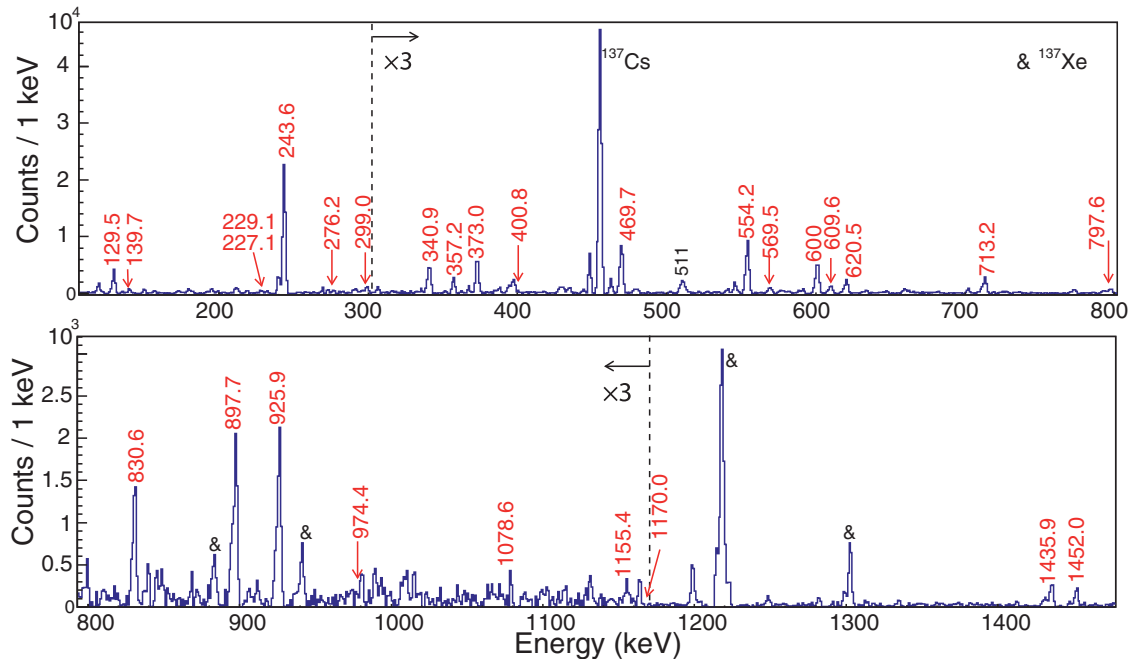


FIG. 4. The $\beta$-gated $\gamma$-ray singles spectrum obtained following the $\beta$ decay of $^{137}$Te, after background subtraction for $Q = 21$. The leftover from the background is from $^{137}$Xe.
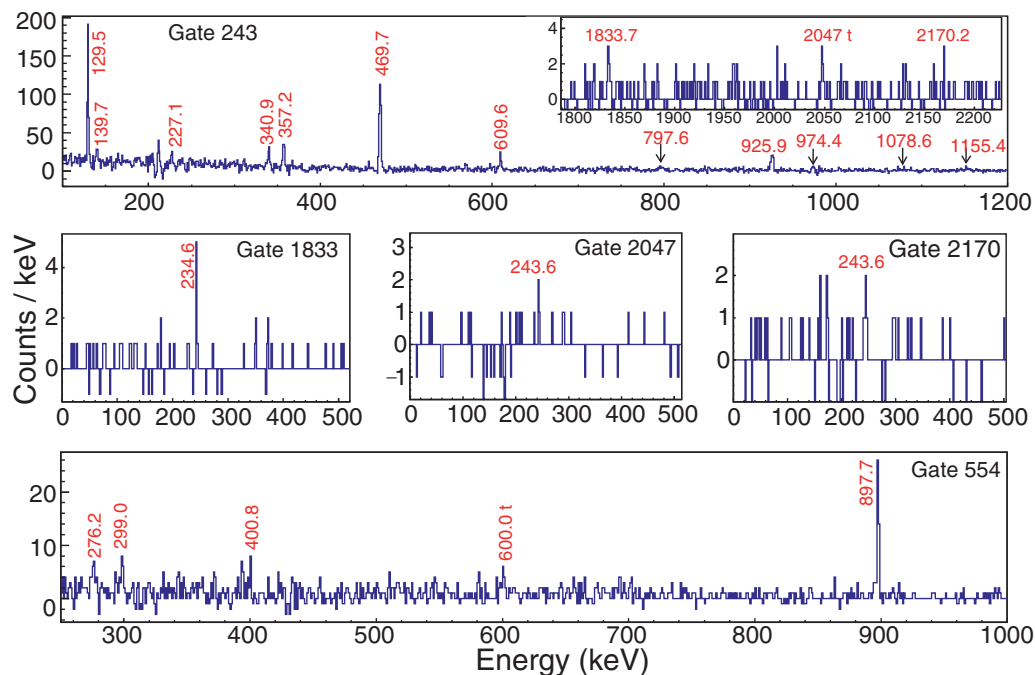
FIG. 5. Coincidence $\gamma$-ray spectra gated on different transitions. All marked peaks (t for tentative) are in mutual coincidence.

229.1 keV line is proposed to be on the top of the 600.6 keV state, establishing a new level with an energy of 830.2 keV. This new level is connected also with the 554.2 keV state by the new 276.2 keV transition. It can also be traced in the coincidence relations depicted in Fig. 5.

The 554.2 keV level was previously observed in the fission reaction studies [8,11], with a single de-excitation by one transition to the ground state (g.s.). One can see from Fig. 5 that the 554.2 keV gated spectrum provides five mutual coincidence lines. The 400.8 keV $\gamma$ transition is known from the previous fission works to connect with the higher-lying $(13/2^+)$ state. The 276.2, 299.0, and 897.7 keV lines are observed for the first time here. The 276.2 keV transition fits the energy difference between the new excited level at 830.2 keV. The 554.2 keV level proves the existence of new connections

with energies of 830.2, 299.1, and 897.7 keV. It provides a piece of evidence in establishing the new excited levels at 853.2 and 1451.9 keV excitation energy. These two levels can also be cross-checked by inspecting their connections to the other levels. The 600 keV transition is marked as tentative, as it is difficult to be distinguished from the deexcitation of the 600.6 keV level to g.s. The 1170.1 keV level is known previously because of its mutual coincidence with the 925.9 and 243.6 keV transitions. Three other transitions deexcite this level as observed in this work, and they are weaker than the 925.9 keV line. The 569.5 keV gated spectrum, illustrated in Fig. 6, shows these coincidence transitions. It suggests that the 569.5 keV line can be placed on top of the 600.6 keV level. Its energy fits well the energy difference between these 1170.1 keV and 600.6 keV states. Therefore, it is assigned to the deexcitation of level 1170.1 keV to level 600.6 keV.

Another previously known transition that we observe here has the energy of 620.5 keV and is assigned to deexcite the 620.5 keV level directly to the g.s., without any connection to the other levels. As we could not identify any coincidence relation with known transitions, we use the time chopper information to obtain its time behavior. The principle of this method is to use the time-energy matrix, by projecting the energy spectrum for every 1 s within the time chopper decay part. Thus, one can trace the transition timing within the correct $T_{1/2}$ of the nucleus of interest. Figure 7(a) shows how the known 243.6 keV transition behaves as an example. The 1435.9 keV transition is assigned as a new transition using these criteria. Figures 7(c) and 7(d) show how transitions from the daughters $^{137}$Xe and $^{137}$Cs behave. Due to their long $T_{1/2}$ the statistics within the decay part remain basically the same for these time projections. This criterion is used to cross-check all the new transitions observed in singles or in gated spectra, and helps to reject any wrongly suspected candidates.
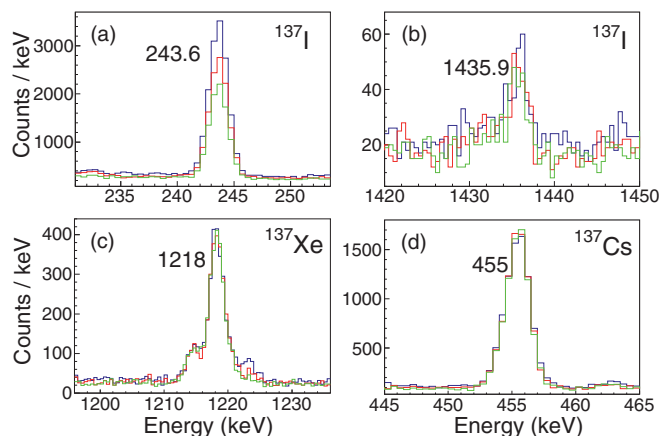


FIG. 6. Coincidence $\gamma$-ray spectra gated on the 247 and 569 keV transitions. All marked peaks are in mutual coincidence.
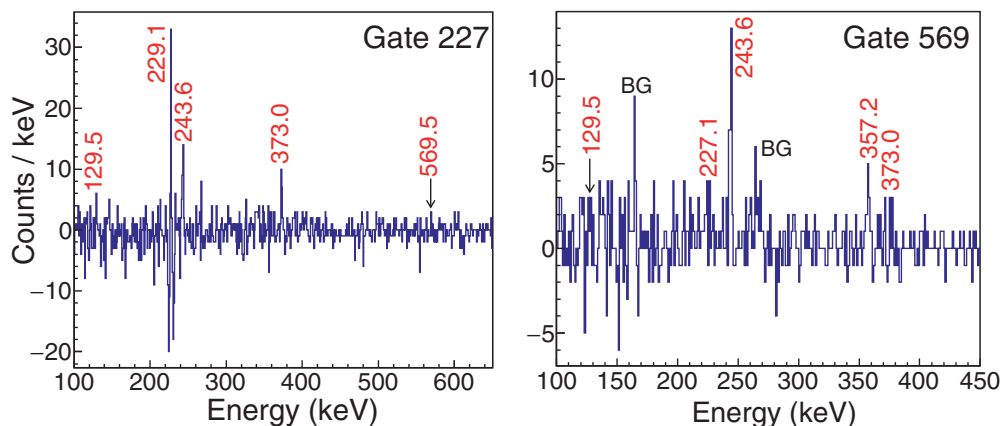
FIG. 7. Energy spectra corresponding to the decay of characteristic $\gamma$ lines in one-second slices. Blue, red and green are for the first, second, and third seconds after closure of the beam chopper, respectively.

To assign new transitions to the level scheme of $^{137}$I we used the following criteria: (a) the correct $T_{1/2}$ behavior; (b) mutual coincidence relations with known or new transitions; (c) the same relative intensity in $Q = 21$ and $Q = 25$ settings (e.g., if two $\gamma$-rays belong to decay the same nucleus, they should have the same population, thus the same intensity between themselves in both settings); (d) not identified in the background. According to these criteria, 17 excited levels could be established in this work with a total of 32 $\gamma$-ray transitions following the $\beta$ decay of $^{137}$Te to $^{137}$I. Among these, we observe for the first time eight new and one tentative levels with eighteen new and two tentative transitions. Table II summarizes the information about the excited levels and $\gamma$ transitions associated with this $\beta$ decay to the $^{137}$I nucleus. The $\gamma$-ray's intensities are normalized to the strongest 243.6 keV transition, and obtained using the background-subtracted full-energy peak areas from the $\beta$-gated $\gamma$-ray spectrum, selecting the time-chopper decay part. The $\beta$ intensity of each level is extracted from the apparent feeding and decaying $\gamma$ transition balance of this particular state. Its log $ft$ value is calculated [25] using $Q(\beta^-) = 7053(9)$ keV from the atomic mass evaluation (AME2020 [26]) and the literature $T_{1/2} = 2.49(5)$ s [12], used in the evaluation.

### C. $^{137}$Te $\beta$ feeding to the $^{137}$I ground state

In order to obtain the $\beta$ feeding to levels in $^{137}$I, both its further decay to $^{137}$Xe and its $P_n$ channel to $^{136}$Xe are considered. As there is no long-lived (e.g., millisecond) isomeric state in $^{137}$I, these are the two branches representing the total g.s. feeding of $^{137}$I. For the $\beta$ decay to $^{137}$Xe, g.s. to g.s. transitions, as well as excited states, are taken into account. This is actually the total number of $^{137}$Te $\beta$ decays (or, alternatively, the total $\gamma$ and $\beta$ feeding intensity to the ground state of $^{137}$I as a result of the $^{137}$Te $\beta$ decay).

We observed 34 excited states and 43 $\gamma$ transitions in $^{137}$Xe populated by the g.s. $\beta$ decay of $^{137}$I, representing about 80% of the known $\gamma$ transition intensities in $^{137}$Xe [13]. We used the well-populated 1302 keV transition with known absolute intensity [$I_\gamma^{abs} = 4.42(44)$%] to obtain the number of $\beta$ decays to $^{137}$Xe. For the $\beta$-$n$ channel of $^{137}$I, the previously known

$P_n$ value is 7.76(14)% [27], compared to the evaluated one of 7.14(23)% [13], and a recent compilation of 7.63(14)% [28]. In this work we did not observe known transitions in $^{136}$Xe.

Combining the above information, it is possible to estimate the decay radiation from the $^{137}$I nucleus, by correcting with the unobserved $P_n$-related $\gamma$ ray. As in the recent evaluation [13] only 100% $\beta$ decay was considered; the $P_n$ branch is now also taken into account to represent the relevant part of the $^{137}$I g.s. decay, using the latest value of 7.76(14)% [27]. Applying the same method to the unknown absolute intensity of an arbitrary transition in $^{137}$I, e.g., the 1435.9 keV line, deexiting the 1435.9 keV level, it is possible to obtain the overall normalization factor for any state. Here it amounts to 0.308(81) and includes the uncertainties of both $I_\beta$ and $I_\gamma$ intensities. This is applicable to the first excited state at 243 keV, decaying by the strongest 243 keV transition. The variation of its $\beta$ intensity from all its $\gamma$ feeders is fully consistent with the propagated uncertainty when considering all other transitions in the $^{137}$I level scheme and results in 13.0(29)% (see Table II). This allows estimating independently the variation in the g.s. feeding of $^{137}$I by assuming the extreme cases: no direct feeding to the g.s. and the maximum $I_\beta$ from the balance of all observed transitions resulting in a total error of 22% relative to the mean value of the intensity.

The simplified way of deducing the intensities, ignoring of the mother-daughter relations of the great granddaughters, is in a very good agreement with the detailed analysis. For these we estimated the initial activity in the three $A = 137$ isotopes Te, I, Xe produced in the reaction and their subsequent decay, ignoring Sb that contributes below 1% to the total activity. This is obtained by fitting the $\beta$ distribution, without considering any $\gamma$ gate, with the full Bateman equations for three subsequent decays [29–31], as well as the periodical activity of the tape as a background. The proportion of the activities for Te and I nuclei is comparable with activity of 53(2)% and 44(2)%, respectively. The Xe activity contributing to the decay is only 4(1)%, at the considered 3 s from the beginning of the cycle. The integrated activity over the 6 s of measuring time is in good agreement with the detected number of Xe decays, derived from its absolute $\gamma$-ray detection.

TABLE II. Excited levels and $\gamma$ transitions in the $\beta$ decay of $^{137}$Te to $^{137}$I. The initial level and its related information are given in the first four columns. The $\gamma$ ray and its relative intensity with respect to the 243.6 keV line are provided in the fifth and sixth columns. Efficiency and conversion corrections are made for the intensities (see text). The last two columns reveal the final level and its spin-parity. The superscript $n$ stands for a new transition, while $u$ marks also an assumption for uniqueness [25].

| $E_i$ (keV) | $J_i^\pi$ | $I_\beta$ (%) | $\log ft$ | $E_\gamma$ (keV) | $I_\gamma + e^-$ | $E_f$ (keV) | $J_f^\pi$ |
|---|---|---|---|---|---|---|---|
| 0.0 | $7/2^+$ | 42(9) | 5.8(1) | | | | |
| 243.6(8) | $5/2^+$ | 13.0(29) | 6.2(1) | 243.6(8) | 100.0(6) | 0 | $7/2^+$ |
| 373.1(7) | $(3/2^+, 5/2^+)$ | 4.6(10) | 6.6(2) | 129.5(7) | 17.4(3) | 243.6 | $5/2^+$ |
| | | | | 373.0(9) | 14.5(3) | 0 | $7/2^+$ |
| 554.2(10) | $9/2^+$ | 7.1(16) | 6.4(1) | 554.2(10) | 33.4(5) | 0 | $7/2^+$ |
| 600.6(6) | $(3/2^+, 5/2^+)$ | 2.5(6) | 6.8(1) | $227.1(7)^n$ | 1.2(1) | 373.1 | $(3/2^+, 5/2^+)$ |
| | | | | 357.2(10) | 5.8(2) | 243.6 | $5/2^+$ |
| | | | | 600.9(10) | 3.8(2) | 0 | $7/2^+$ |
| 620.5(10) | $9/2^+, 11/2^+$ | 2.6(6) | 6.8(1) | 620.5(10) | 8.3(2) | 0 | $7/2^+$ |
| 713.5(7) | $(7/2^+)$ | 15.0(33) | 6.0(1) | 340.9(11) | 12.7(2) | 373.1 | $(3/2^+, 5/2^+)$ |
| | | | | 469.7(9) | 24.6(4) | 243.6 | $5/2^+$ |
| | | | | 713.2(12) | 12.8(3) | 0 | $7/2^+$ |
| $830.2(6)^n$ | $(5/2^+, 9/2^+)$ | 1.5(3) | 7.0(1) | $229.1(7)^n$ | 1.2(1) | 600.6 | $(3/2^+, 5/2^+)$ |
| | | | | $276.2(5)^n$ | 0.3(1) | 554.2 | $9/2^+$ |
| | | | | $830.6(11)^n$ | 3.4(2) | 0 | $7/2^+$ |
| $853.2(7)^n$ | $(5/2^+, 9/2^+)$ | 1.6(4) | 7.0(1) | $139.7(6)^n$ | 1.2(1) | 713.5 | $(7/2^+)$ |
| | | | | $299.0(11)^n$ | 2.1(1) | 554.2 | $9/2^+$ |
| | | | | $609.6(10)^n$ | 1.9(1) | 243.6 | $5/2^+$ |
| 955.0(12) | $11/2^+, 13/2^+$ | 0.3(1) | $7.6–9.6^u$ | 400.8(7) | 1.1(1) | 554.2 | $9/2^+$ |
| 1170.1(6) | $(7/2^+)$ | 2.9(7) | 6.6(1) | $569.5(9)^n$ | 1.5(1) | 600.6 | $(3/2^+, 5/2^+)$ |
| | | | | $797.6(10)^n$ | 2.0(1) | 373.1 | $(3/2^+, 5/2^+)$ |
| | | | | 925.9(12) | 5.2(2) | 243.6 | $5/2^+$ |
| | | | | $1170.0(7)^n$ | 0.7(1) | 0 | $7/2^+$ |
| $1218.0(11)^n$ | $(3/2^+, 9/2^+)$ | 0.3(1) | 7.5(1) | $974.4(8)^n$ | 1.1(1) | 243.6 | $5/2^+$ |
| $1399.0(11)^n$ | $(3/2^+, 11/2^+)$ | 0.2(1) | $7.7–9.6^u$ | $1155.4(8)^n$ | 0.6(1) | 243.6 | $5/2^+$ |
| $1435.9(9)^n$ | $(5/2^+, 9/2^+)$ | 0.8(2) | 7.1(1) | $1435.9(9)^n$ | 2.6(2) | 0 | $7/2^+$ |
| $1451.9(7)^n$ | $(7/2^+)$ | 2.5(6) | 6.6(1) | $600^f$ | | 853.2 | $(5/2^+, 9/2^+)$ |
| | | | | $897.7(9)^n$ | 4.7(2) | 554.2 | $9/2^+$ |
| | | | | $1078.6(8)^n$ | 1.0(1) | 373.1 | $(3/2^+, 5/2^+)$ |
| | | | | $1452.0(11)^n$ | 2.5(2) | 0 | $7/2^+$ |
| $2077.3(14)^n$ | $(3/2^+, 11/2^+)$ | 0.1(1) | $7.7–9.5^u$ | $1833.7(11)^n$ | 0.3(1) | 243.6 | $5/2^+$ |
| $2290.6(14)^f$ | | | | $2047^f$ | | 243.6 | $5/2^+$ |
| $2413.8(12)^n$ | $(3/2^+, 9/2^+)$ | 0.2(1) | 7.3(1) | $2170.2(9)^n$ | 0.6(1) | 243.6 | $5/2^+$ |

Taking into account the above analysis, the final number $I_\beta$ of g.s. feeding and its variation are reported in Table II. This is reflected also in the experimental $\log ft$ uncertainties of particular levels as a systematic error, while the statistical errors contribute to below or around the percent level in this measurement. It may be noted also that we corrected all $\gamma$ transitions in $A = 137$ for conversion [32]. While in some of these transitions, such as the one at 243.6 keV, the multipolarity comes from previous measurements [11,33], for the others possible $M1$ and $E2$ assumptions are made. Most of these transitions are weak in intensity and their proportion is found to be minor. However, for two relevant $\gamma$ rays of 129.5 and 139.7 keV, the conversion factors assuming the four different combinations change the relative $I_\beta$ of the level. For example, for the 243.6 keV level, the $I_\beta$ uncertainty may increase from 13.0(29) to 13.0(37). This is relevant also for the 373.1, 713.5, and 853.2 keV levels.

Note that such strong feeding to the g.s. as observed in this measurement is fully consistent with the g.s. assignment of this level and other states in the level scheme, discussed in Sec. III D. It is the strongest $\beta$-decay channel from the $7/2^-$ g.s. of the mother $^{137}$Te, feeding to the $7/2^+$ g.s. $^{137}$I of the daughter (type $\nu f_{7/2} \rightarrow \pi g_{7/2}$). This was suggested from systematics [13], previous measurements [11,12], and shell-model calculations (see Sec. IV).

### D. Level scheme and spin-parity assignments

For $7/2^-$ g.s. spin-parity of the parent nucleus suggested previously [11,12,33], only the low-spin states are expected to be observed in its $\beta$ decay, taking into account the predominant forbidden nature of these transitions. The g.s. spin-parity of the $^{137}$I daughter as $7/2^+$ was established earlier and is completely consistent with our work here (see Sec. IV A for details). For the 620.5 keV state, the spin-parity of $11/2^+$

was set because of the deduced $E2$ transition multipolarity of the 620.5 keV $\gamma$ ray in the spontaneous fission data [11]. In that study, the angular correlations of this line were regarded with respect to the 333.9 keV line, connecting the suggested $13/2^+$ level at 955.0 with the proposed $11/2^+$ level, and it was assumed to be of an $M1 + E2$ type.

The 620.5 keV state observed in this work represents a single transition to the ground state. However, we could not detect any coincident transitions to represent feeders from above. Thus, its intensity should be mostly coming in direct $\beta$ feeding. Such a scenario would not be entirely consistent with an earlier proposed spin-parity of $11/2^+$ and $\log ft$ value of 6.8(1) evaluated in this work, therefore according to our data $\Delta J < 2$ possibility is not be excluded. For example, if the presumed $11/2^+$ level would be a $9/2^+$ candidate, the 620.5 keV transition may have some mixing and this would not conflict with several deviations from the theoretical angular correlation coefficients from the previous observation in Ref. [11]. Such a scenario would include the margin in the $\beta$ intensity, observed in this experiment, and this may be also suggested for the 620.5 keV level. We note that, as the data are not free from the Pandemonium effect, the assignment based on $\log ft$ values is only indicative.

The 554.2 keV [13] state was set to $9/2^+$ based on the suggested mixed $M1 + E2$ multipolarity of the 554.2 keV transition, observed in Ref. [11], with respect to the 400.8 keV transition. Both were placed in the level scheme in coincidence, which we indeed also observe in Fig. 5. Similarly, if the 400.8 keV transition orignates from an $11/2^+$ instead of the $13/2^+$, suggested for the 955.0 keV level, possible mixing due to some deviations in angular distribution, polarization data, or alternation of spins may need to be assumed. In this experimental data, due to visible $I_\beta$ intensity and relatively well fitting $\log ft$ values, the previously assigned $11/2^+$ and $13/2^+$ states are now given possible alternative assignments in the level scheme, shown in Fig. 8 and Table II.

As we detect the 554.2 keV transition as the second strongest, relative to that of the first excited state (also previously identified with spin-parity of $5/2^+$ [12]), this gives quite some certitude for the spin of the originating state. It does well fit the spin-parity of $7/2^+$ for the g.s. and is in a very good agreement with our shell-model (SM) expectations (see Sec. IV), placing the first $9/2^+$ state at 554.2 keV excitation energy. Furthermore, looking at the $I_\beta$ and $\log ft$ values for the 554.2 keV level, the $5/2^+$ possibility cannot be completely excluded. This tendency actually comes from the fact that the 554.2 keV transition is mostly of an $M1$ type, mixed with an $E2$ multipolarity. Therefore, the required $\Delta J = 1$ branch would connect similarly strongly a $5/2^+$ state to the $7/2^+$ ground state. Note, that this would somewhat deviate from the predicted second $5/2^+$ state, which may be theoretically expected to appear much below the excitation energy of the first $9/2^+$ state. As observed, such a state is populated directly and relatively strongly in the $7/2^-$ g.s. $\beta$ decay.

The next candidate for a second $(7/2^+)$ state is the previously observed 713.5 keV state, deexciting by three $\gamma$ transitions, that we also observe, with the strongest one connecting to the 243.6 keV level with a spin-parity of $5/2^+$ [11,12]. Its experimental $I_\beta$ and $\log ft$ also indicate a $(7/2^+)$ assignment. However, such identification would be somewhat in variance with the SM prediction that expects the second $7/2^+$ level at 571 keV excitation energy, while the third $7/2^+$ state is calculated at 774 keV (see Sec. IV). Although they all are predicted with the same configuration, there is no clear reason why they would be compressed, except for the possibility of unaccounted mixing in the configuration of these states. The third candidate for this spin-parity, according to our data, is at an excitation energy of 1170.1 keV. This is very probable and matches the findings of Ref. [12] to our data. We detect three additional transitions deexiting this level (see Fig. 8). It must have been among the strongest ones observed in that first $\beta$-decay study of $^{137}$Te. The proposed spin-parities as $5/2^+$ and $7/2^+$ would be the favored ones from the $7/2^-$ g.s. of the mother nucleus, and this is fully consistent with our conclusions.

The two levels at 830.2 and 853.2 keV have similar $I_\beta$ and $\log ft$ values. These $\beta$ feeding intensities are lower than what would be expected for a spin-parity of $7/2^+$ for any of these levels. Besides, their interconnecting transitions to the lower-lying $5/2^+$ and $9/2^+$ states make such possible $7/2^+$ assignment less adequate. Therefore, we propose the $(5/2^+, 9/2^+)$ alternatives for the spin-parities of the two states. This would agree with the SM results for $9/2^+$ and be underestimated for a $5/2^+$ state, while the third $7/2^+$ and $3/2^+$ states, expected in the vicinity of 774 and 900 keV, require a different experimental branching.

The next level, which experimentally has a strong $I_\beta$ feeding and can be a $(7/2^+)$ state, is located at 1170.1 keV. It was observed previously also as a strong decay branch and, in addition, corresponds well to the fourth $7/2^+$ state, predicted at 1085 keV. The state at 1451.9 keV, which has similar characteristics, may have the same origin, thus is also proposed as a $(7/2^+)$ level. Although the $(5/2^+)$ possibility cannot be completely excluded, it would require more data to search for feeding branches that we could not observe. Interestingly, the five states we suggest with a spin-parity of $5/2^+$ or $7/2^+$ ($E_x < 1.2$ MeV), being the strongest fed, were listed in the level scheme, through left unassigned in Ref. [12].

In the data presented here, it can be seen that four similar new excited states at 830.2, 853.2, 1435.9, and 1451.9 keV are established. According to their possible de-excitation transition multipolarities, the spin-parities are consistent with the earlier proposed $(9/2^+)$ spin-parity. Although indicative, due to the relatively low $\log ft$ value, a $(5/2^+)$ possibility may be added or even $(7/2^+)$ for the latter one.

Some spin-parity assignments suggested previously [11], were based on the possible proton-neutron SM configuration (see Sec. IV). A possible $\beta$ decay of $^{137}$Te to $^{137}$I is expected to primarily originate from the conversion of a neutron from the $f_{7/2}$ orbital into a proton in the $g_{7/2}$ (or $d_{5/2}$) orbital by a first-forbidden transition, in agreement with the spin-parity of $^{137}$Te g.s. of $7/2^-$. The feeding to the g.s. of the daughter $^{137}$I with $\log ft = 5.8(1)$ and maximal $I_\beta$ value of 42(9)% indicates that it proceeds by a first-forbidden nonunique transition with $\Delta J = 0$ and $\Delta \pi = -1$ [34]. This suggests spin-parity
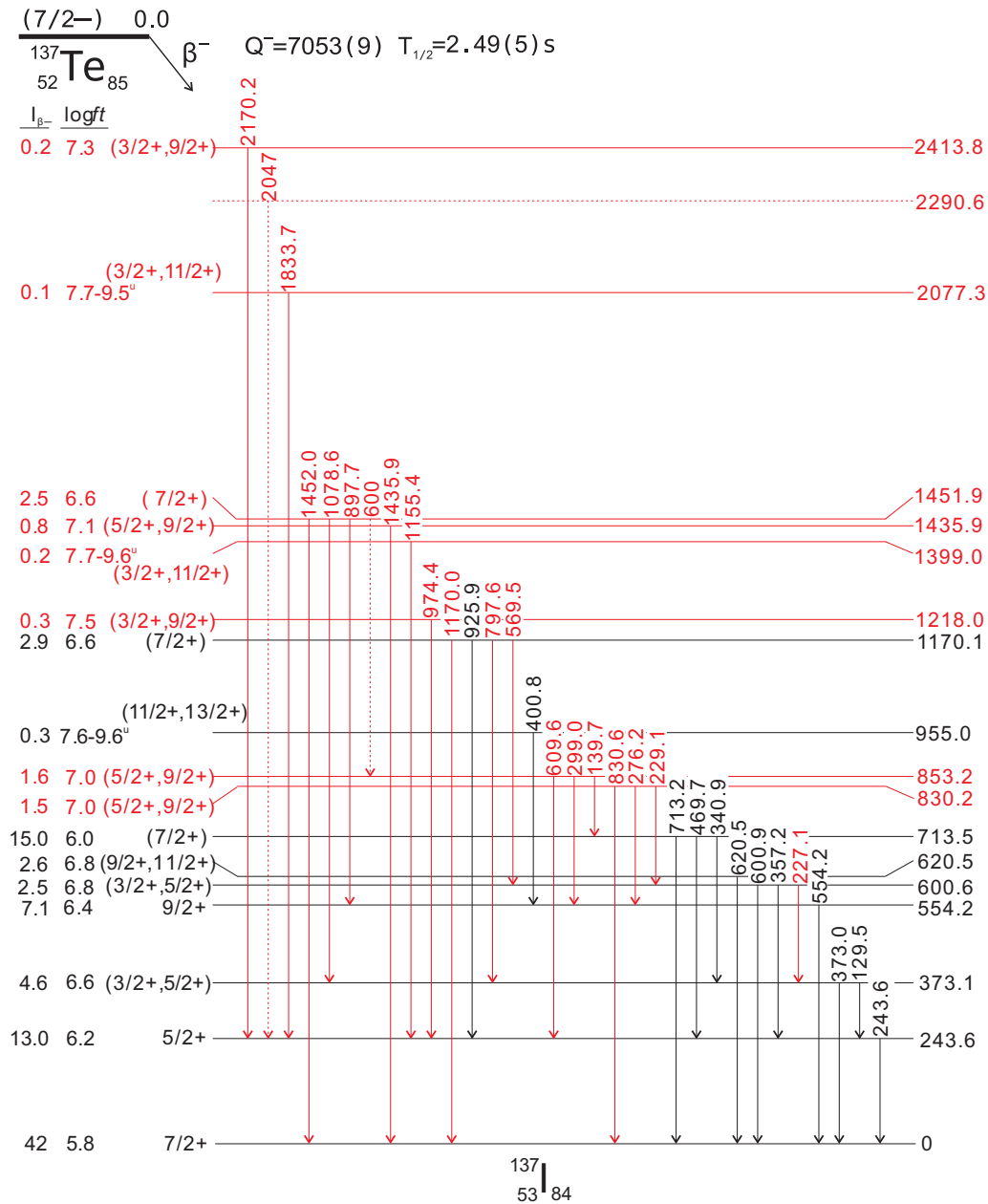
FIG. 8. The proposed level scheme of $^{137}$I obtained from $\beta$ decay of $^{137}$Te. The new levels and transitions are in red, tentative transitions are shown with dotted lines. The $Q(\beta^-)$ of $^{137}$Te is taken from Ref. [26]. For the levels marked with (*), some assumption for uniqueness may be possible (see text, Table II).

of $7/2^+$, in agreement with the spin-parity suggested from systematics [12,13]. Three more levels with suggested spin-parity of $(7/2^+)$ could be identified in the level scheme with log $ft$ values between 6.0 and 6.6.

Other levels candidates, e.g., with a log $ft$ of 6.8(1) and a smaller $I_\beta$ of 2.4–2.9, possibly correspond to $\Delta J = 1, 2$; for these, spin-parity of $(3/2^+, 5/2^+)$ would be more appropriate. For about six levels with log $ft$ ranging from 6.2 to 7.1, we propose the spin-parity of $(5/2^+)$ to be the most suitable candidate. In addition, based on the $I_\beta$ branching, possible spins, and multipolarities it may be assumed that some levels

are candidates for $\Delta J = 2$, which suggests some uniqueness when appropriate, as marked in Table II.

The proposed level scheme from this work is illustrated in Fig. 8. Nine new levels (with one tentative among them) with eighteen new transitions (with two tentative) are added to the revised previous knowledge. The tentative $\gamma$ rays with 600 and 2047 keV energy which are hardly distinguishable in the $\beta$-delayed $\gamma$-ray spectrum of $^{137}$I are placed as they appear in the gated spectrum and, moreover, fit the energy differences between already established levels.

main configurations
— $\nu f_{7/2}^2 \pi g_{7/2}^3$
— $\nu f_{7/2}^2 \pi g_{7/2}^2 d_{5/2}$

$(3/2^+,9/2^+)$ 2413
2290
$(3/2^+,11/2^+)$ 2077

$3/2^+$ 2339
$3/2^+$ 2219
$3/2^+$ 2054

$3/2^+$ 1843
$3/2^+$
$3/2^+$
$3/2^+$

$11/2^+$
$9/2^+$ $11/2^+$
$9/2^+$ $11/2^+$

$(3/2^+,11/2^+)$ $(5/2^+,9/2^+)$ $(7/2^+)$ 1451
1399 1435
$(3/2^+,9/2^+)$ 1218
$(7/2^+)$ 1170

$3/2^+$ 1404
$5/2^+$ 1384
$3/2^+$ 1171
$7/2^+$ 1269 $9/2^+$
$7/2^+$ 1085
$5/2^+$ 1037
$7/2^+$

$9/2^+$ $11/2^+$ $13/2^+$
1267
$9/2^+$ $11/2^+$ 1008
$13/2^+$ 960

11/2^+,13/2^+ 955
$(5/2^+,9/2^+)$ 853
830 $(7/2^+)$ 713
$(3/2^+,5/2^+)$ 600 $9/2^+,13/2^+$
$(9/2^+)$ 554 620
$(3/2^+,5/2^+)$ 373
$5/2^+$ 243
$7/2^+$ 0

$3/2^+$
$5/2^+$ 931
$3/2^+$ 464
$3/2^+$ 288 $5/2^+$
$5/2^+$ 188
$5/2^+$
$7/2^+$ 0

$9/2^+$ 757
$7/2^+$ 571 $9/2^+$ 567
$11/2^+$ 588

exp                                    $^{137}_{53}\text{I}_{84}$                                    SM
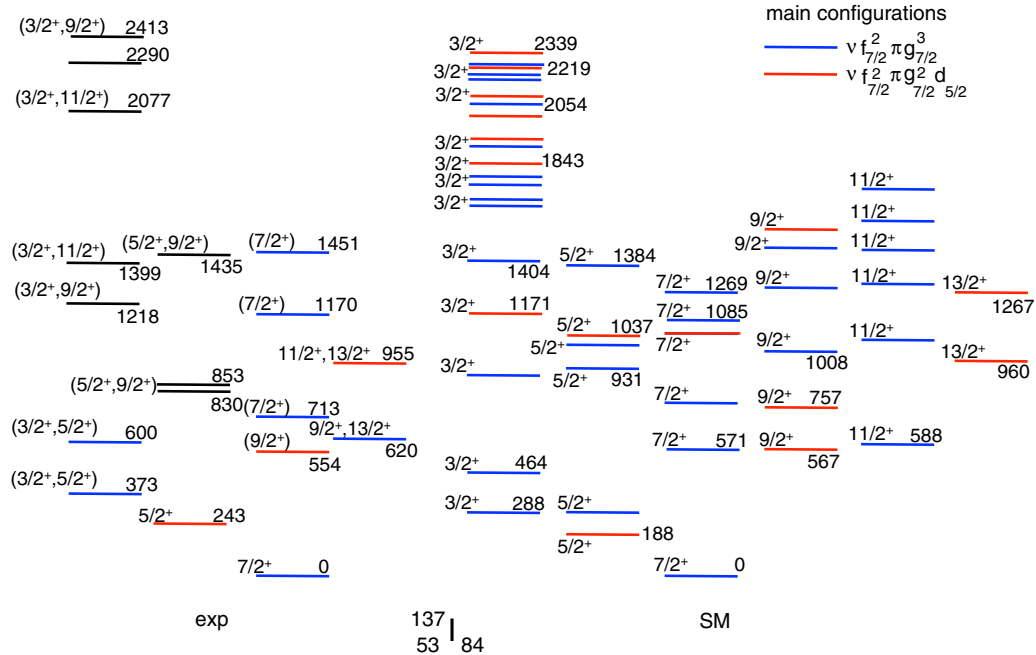
FIG. 9. Experimental levels in $^{137}$I compared to the theoretical shell-model (SM) calculations. The color code indicates the main theoretical configurations and some of the possible experimental correspondences.

### E. $P_n$ branch

Since the $S_n$ of the $^{137}$I daughter is 4882(16) keV, within the $Q_\beta$ window of $Q_\beta = 7053(9)$ keV [26,35], $\beta$-delayed neutron emission is possible for the decay of the $^{137}$Te nucleus.

To obtain the $\beta$-delayed neutron emission probability, $P_n$, of $^{137}$Te, we consider known $\gamma$ transitions in the $\beta n$ daughter $^{136}$I [7], selected with the same criteria as for transitions in $^{137}$Te. Only one state at 87.3(7) keV with a single transition to the g.s. is observed in this work. The resulting $P_n$ amounts to 2.63(85)%, but since additional weaker transitions that remained unobserved cannot be excluded, this number represents actually a lower limit. Nonetheless, comparing to the latest literature value of $P_n = 2.6(3)\%$ and the evaluated database value of $P_n = 2.91(16)\%$ in Ref. [28], it appears that the 87.3 keV transition captures most of the $\beta n$ intensity.

## IV. SHELL-MODEL CALCULATIONS AND DISCUSSION

The experimental results are compared to theoretical calculations from large-scale shell-model (SM) calculations. The $r4h$–$r5i$ model space with the $^{132}$Sn nucleus as a core is used. The model-space thus consists of the entire major shell $1f_{7/2}, 0h_{9/2}, 1f_{5/2}, 2p_{3/2}, 2p_{1/2}, 0i_{13/2}$ orbitals for neutrons and $0g_{7/2}, 1d_{5/2}, 1d_{3/2}, 2s_{1/2}, 0h_{11/2}$ orbitals for protons. Single-particle energies for neutrons and protons are taken from experimentally known data on $^{133}$Sn and $^{133}$Sb nuclei [36]. The $0i_{13/2}$ neutron and $2s_{1/2}$ proton orbital energies are inferred from Refs. [37,38], respectively. The N3LOP effective interaction [39] is used in this work. Several articles already successfully described the spectroscopic properties and collectivity of nuclei in the region beyond $^{132}$Sn, e.g.,

Refs. [7,8,39–41]. The diagonalization of the considered system is achieved using the NATHAN shell-model code [42]. In this work, up to several excited states for the spin-parity and energy range of interest are calculated and compared to the proposed spin-parity assignments from the experiment in Fig. 9; the important main configurations for the positive (+) parity states are listed in Table III.

For the states of interest, illustrated in Fig. 9, also the main SM configurations are noted. The probable correspondence, whenever possible, may also be seen (with the color code).

It is interesting to remark immediately that for these states the configuration is dominated by the proton configurations, especially the presence of the $d_{5/2}$ proton in the very close vicinity of the $g_{7/2}$ proton, inferred from the main occupation of these orbitals. Almost no neutron excitations are found to take place in the detailed analysis of the wave functions for the examined states, even for the highest excitation energy. Note that reviewing higher-lying states would not be relevant to the observed experimental data. The details of the main configurations for $^{137}$I may be traced for the computed states in Table III. This is certainly very different from the observed sequences in the $^{136}$I neighbor, where various neutron excitations could be seen [7], including some moderate $\nu i_{13/2}$ occupation (see, e.g., Fig. 13 in that paper). Such behavior may be attributed to the proximity of the $N = 82$ closed shell, in the former case, to the transition with the extra neutrons from an odd-odd to an odd-even system, and finally to its structure.

As it can be seen from Table III, the purity of the two main configurations in the low-energy states of $^{137}$I is not small and, therefore, the other contributions appear with relatively minor weight in the wave functions. We present these results in accordance with the excited states that are candidates for

TABLE III. Main wave-function compositions for the positive (+) parity states of interest as predicted by the SM calculations for $^{137}$I.

| $J_i^\pi$ | Configuration I | % | Configuration II | % |
|---|---|---|---|---|
| $3/2_1^+$ | $\pi(g_{7/2}^3)\nu(f_{7/2}^2)$ | 15 | $\pi(g_{7/2}d_{5/2}^2)\nu(f_{7/2}^2)$ | 11 |
| $3/2_2^+$ | $\pi(g_{7/2}^3)\nu(f_{7/2}^2)$ | 13 | $\pi(g_{7/2}^2d_{5/2})\nu(f_{7/2}^2)$ | 11 |
| $3/2_3^+$ | $\pi(g_{7/2}^3)\nu(f_{7/2}^2)$ | 26 | $\pi(g_{7/2}^2d_{3/2})\nu(f_{7/2}^2)$ | 11 |
| $3/2_4^+$ | $\pi(g_{7/2}^2d_{5/2})\nu(f_{7/2}^2)$ | 17 | $\pi(d_{5/2}^3)\nu(f_{7/2}^2)$ | 12 |
| $3/2_5^+$ | $\pi(g_{7/2}^3)\nu(f_{7/2}^2)$ | 42 | $\pi(g_{7/2}^2d_{5/2})\nu(f_{7/2}^2)$ | 7 |
| $3/2_6^+$ | $\pi(g_{7/2}^3)\nu(f_{7/2}^2)$ | 34 | $\pi(g_{7/2}^2d_{5/2})\nu(f_{7/2}^2)$ | 12 |
| $3/2_7^+$ | $\pi(g_{7/2}^3)\nu(f_{7/2}^2)$ | 39 | $\pi(g_{7/2}d_{5/2}^2)\nu(f_{7/2}^2)$ | 13 |
| $3/2_8^+$ | $\pi(g_{7/2}^3)\nu(f_{7/2}^2)$ | 17 | $\pi(g_{7/2}^2d_{5/2})\nu(f_{7/2}^2)$ | 17 |
| $3/2_9^+$ | $\pi(g_{7/2}^3)\nu(f_{7/2}^2)$ | 31 | $\pi(g_{7/2}^2d_{5/2})\nu(f_{7/2}^2)$ | 9 |
| $3/2_{10}^+$ | $\pi(g_{7/2}^2d_{5/2})\nu(f_{7/2}^2)$ | 27 | $\pi(g_{7/2}^3)\nu(f_{7/2}^2)$ | 12 |
| $5/2_1^+$ | $\pi(g_{7/2}^2d_{5/2})\nu(f_{7/2}^2)$ | 41 | $\pi(g_{7/2}^2d_{5/2})\nu(f_{7/2}p_{3/2})$ | 8 |
| $5/2_2^+$ | $\pi(g_{7/2}^3)\nu(f_{7/2}^2)$ | 33 | $\pi(g_{7/2}^2d_{5/2})\nu(f_{7/2}^2)$ | 9 |
| $5/2_3^+$ | $\pi(g_{7/2}^3)\nu(f_{7/2}^2)$ | 26 | $\pi(g_{7/2}d_{5/2}^2)\nu(f_{7/2}^2)$ | 12 |
| $5/2_4^+$ | $\pi(g_{7/2}^3)\nu(f_{7/2}^2)$ | 32 | $\pi(g_{7/2}d_{5/2}^2)\nu(f_{7/2}^2)$ | 17 |
| $5/2_5^+$ | $\pi(g_{7/2}^2d_{5/2})\nu(f_{7/2}^2)$ | 23 | $\pi(g_{7/2}^3)\nu(f_{7/2}^2)$ | 16 |
| $5/2_6^+$ | $\pi(g_{7/2}^3)\nu(f_{7/2}^2)$ | 30 | $\pi(g_{7/2}^2d_{5/2})\nu(f_{7/2}^2)$ | 22 |
| $7/2_1^+$ | $\pi(g_{7/2}^3)\nu(f_{7/2}^2)$ | 31 | $\pi(g_{7/2}d_{5/2}^2)\nu(f_{7/2}^2)$ | 19 |
| $7/2_2^+$ | $\pi(g_{7/2}^3)\nu(f_{7/2}^2)$ | 18 | $\pi(g_{7/2}d_{5/2}^2)\nu(f_{7/2}^2)$ | 17 |
| $7/2_3^+$ | $\pi(g_{7/2}^3)\nu(f_{7/2}^2)$ | 23 | $\pi(g_{7/2}^2d_{5/2})\nu(f_{7/2}^2)$ | 22 |
| $7/2_4^+$ | $\pi(g_{7/2}^2d_{5/2})\nu(f_{7/2}^2)$ | 29 | $\pi(g_{7/2}^3)\nu(f_{7/2}^2)$ | 22 |
| $7/2_5^+$ | $\pi(g_{7/2}^3)\nu(f_{7/2}^2)$ | 40 | $\pi(g_{7/2}^2d_{5/2})\nu(f_{7/2}^2)$ | 11 |
| $7/2_6^+$ | $\pi(g_{7/2}^3)\nu(f_{7/2}^2)$ | 35 | $\pi(g_{7/2}^2d_{5/2})\nu(f_{7/2}^2)$ | 16 |
| $9/2_1^+$ | $\pi(g_{7/2}^2d_{5/2})\nu(f_{7/2}^2)$ | 17 | $\pi(g_{7/2}^3)\nu(f_{7/2}^2)$ | 12 |
| $9/2_2^+$ | $\pi(g_{7/2}^2d_{5/2})\nu(f_{7/2}^2)$ | 26 | $\pi(g_{7/2}^2d_{5/2})\nu(f_{7/2}p_{3/2})$ | 13 |
| $9/2_3^+$ | $\pi(g_{7/2}^3)\nu(f_{7/2}^2)$ | 44 | $\pi(g_{7/2}d_{5/2}^2)\nu(f_{7/2}^2)$ | 10 |
| $9/2_4^+$ | $\pi(g_{7/2}^3)\nu(f_{7/2}^2)$ | 46 | $\pi(g_{7/2}d_{5/2}^2)\nu(f_{7/2}^2)$ | 10 |
| $9/2_5^+$ | $\pi(g_{7/2}^3)\nu(f_{7/2}^2)$ | 33 | $\pi(g_{7/2}d_{5/2}^2)\nu(f_{7/2}^2)$ | 11 |
| $9/2_6^+$ | $\pi(g_{7/2}^2d_{5/2})\nu(f_{7/2}^2)$ | 28 | $\pi(g_{7/2}^2d_{5/2})\nu(f_{7/2}^2)$ | 12 |
| $11/2_1^+$ | $\pi(g_{7/2}^3)\nu(f_{7/2}^2)$ | 23 | $\pi(g_{7/2}d_{5/2}^2)\nu(f_{7/2}^2)$ | 15 |
| $11/2_2^+$ | $\pi(g_{7/2}^3)\nu(f_{7/2}^2)$ | 20 | $\pi(g_{7/2}d_{5/2}^2)\nu(f_{7/2}^2)$ | 15 |
| $11/2_3^+$ | $\pi(g_{7/2}^3)\nu(f_{7/2}^2)$ | 31 | $\pi(g_{7/2}^2d_{5/2})\nu(f_{7/2}^2)$ | 16 |
| $11/2_4^+$ | $\pi(g_{7/2}^3)\nu(f_{7/2}^2)$ | 51 | $\pi(g_{7/2}d_{5/2}^2)\nu(f_{7/2}^2)$ | 10 |
| $11/2_5^+$ | $\pi(g_{7/2}^3)\nu(f_{7/2}^2)$ | 30 | $\pi(g_{7/2}^2d_{5/2})\nu(f_{7/2}^2)$ | 22 |
| $11/2_6^+$ | $\pi(g_{7/2}^3)\nu(f_{7/2}^2)$ | 24 | $\pi(g_{7/2}^2d_{5/2})\nu(f_{7/2}^2)$ | 23 |
| $13/2_1^+$ | $\pi(g_{7/2}^2d_{5/2})\nu(f_{7/2}^2)$ | 20 | $\pi(g_{7/2}^3)\nu(f_{7/2}^2)$ | 13 |
| $13/2_2^+$ | $\pi(g_{7/2}^2d_{5/2})\nu(f_{7/2}^2)$ | 31 | $\pi(g_{7/2}^3)\nu(f_{7/2}^2)$ | 14 |

the experimentally populated spin-parity. In the table, we give up to ten excited states for the $3/2^+$ candidates for populated states at intermediate energy, and up to six excited states, as relevant, for the spin-parities $5/2^+$, $7/2^+$, $9/2^+$, $11/2^+$, and $13/2^+$ (see Fig. 9). Note that the neutron excitation to the $\nu p_{3/2}$ orbital is applicable only in a very few cases. The proton excitations containing the $\pi d_{5/2}$ orbital show clearly a competition with the $\pi g_{7/2}$ orbital for excited states and are also the second important contribution (with about 20%) in the $7/2^+$ g.s. of $^{137}$I.

Another important point is the very small contribution of the $\nu h_{9/2}$ orbital in the wave function of the $7/2^-$ g.s. of the mother $^{137}$Te nucleus. The presence of this $\nu h_{9/2}$ component and its decay to a state with $\pi h_{11/2}$ component in the daughter is the main responsible transition for a Gamow-Teller (GT) strength at the beginning of this major shell. In the neighboring $^{136}$I case, several $1^+$ states originating from this main configuration are populated, with one very strong branch, as predicted by the SM, at about 2 MeV excitation energy [7]. A similar range was recently suggested also for $^{138}$I in Ref. [23]. Here, for $A = 137$, the $\nu h_{9/2}$ component is really minor with a theoretically calculated proportion of only 2.5%. Note that, while present in $A = 136$ with about 10%, it is completely blocked, e.g., for $^{135}$I. It is worth highlighting that, for $A = 140$ of the same isotopic chain ($^{140}$I), this probability is again enhanced with respect to $A = 137$. This is based on the more mixed g.s. configuration on one side, and due to the lowered excitation energy of the GT states themselves, on the other, as can be seen from the results in Ref. [43].

While reporting on the first excited states in the $^{137}$Te mother nucleus, in Ref. [33], some $\nu h_{9/2}(f_{7/2}^2)$ contributions account for, e.g., the yrast $9/2^-$ states, including the g.s. together with the three-valence $\nu f_{7/2}^3$ configuration. These, as well as core vibrations coupled to them, were suggested to originate the $3/2^-$ and $5/2^-$ states; however, they were not observed in the same study, while the position of these states is relevant in the situation of $^{137}$Te nucleus. These states could be seen only in the more recent $\beta$ decay of $^{137}$Sb $\rightarrow$ $^{137}$Te [23], where the first negative parity states expected with such configurations are found at relatively high energy. Such states are not among those identified in our $\beta$-decay scheme. It could, therefore, be concluded that at $A = 137$ no allowed branch $\nu h_{9/2} \rightarrow \pi h_{11/2}$ could be experimentally observed. As such contribution to the expected configurations is minor also in the examined $^{137}$Te $\rightarrow$ $^{137}$I study here, and none of the excited states seem to present such a strong transition branching, we give similar conclusions for this odd-$A$ $\beta$ decay.

### A. The $7/2^-$ g.s. of $^{137}$Te

The g.s. spin-parity of the $\beta$-decaying $^{137}$Te nucleus can rather firmly be set to $7/2^-$ based on the experimental findings of this work, log $ft$ values in the $A = 137$ I daughter, and the very strong branch to its $7/2^+$ g.s., together with all findings of the previous works on this nucleus. The direct g.s. to g.s. feeding is also relatively strong in this $\beta$ decay with about 42%. It behaves completely analogously to the $A = 135$ case with similar experimental strength [12], from which similar spin-parities can be concluded.

The g.s. of $^{137}$Te was suggested with quite some certitude in Ref. [11], based on the observation of a large part of its yrast scheme [up to spin-parity of $(33/2^+)$]. Also multipolarity of several transitions connecting with the g.s. and SM calculations based on the Kuo-Herling (KH5082) [44] interaction reasonably well describe $^{137}$I, like the one-proton coupling to the $^{136}$Te nucleus. The perfect match of this assignment for the $^{137}$I ($Z = 53$, $N = 84$) isotope to the systematics of heavier-$Z$ Cs, La isotone nuclei is found in a followup fission work [45]. There, the entire excitation scheme could be built

in complete analogy to the $^{139}$Cs ($Z = 55$, $Z = 84$) isotone and in agreement with the data on other $N = 85$ isotones [46]. These excitations are found also to be well described by the two-body CD-Bonn SM interaction using experimental single-particle energies from $^{133}$Sb and $^{133}$Sn nuclei [1].

Both mother and daughter $A = 137$ g.s. spin-parity assignments are in good agreement also with our SM calculations using the N3LOP effective interaction. They predict the $7/2^-$ state to be the $^{137}$Te g.s.. It was already reported that this prediction for the lowest state with the largest probability (>50%) as a single-neutron state is fully consistent with the Napoli SM interaction [23].

It is worth noting that similar predictions were given also in earlier works [33], where the $7/2^-$ assignment was compared to the systematics of the heavier isotones (up to $Z = 64$) and it was concluded that it is the best choice for this $Z = 52$ nucleus. Also, it is quoted in Ref. [33] that this would suit the nonobservation (in their data) of candidates for the $3/2^-$ and $5/2^-$ states for this nucleus. These candidates could only be tentatively suggested from $\beta$ decay to $^{137}$Te. The $(5/2^-)$ state is set at an excitation energy of 61.8 keV [23]. At least 1136.6 keV is suggested for a possible $(3/2^-)$ state, despite this resulting in some variance with the SM theory. For example, both N3LOP and Napoli SM interactions predict these two states as first excited states in $^{137}$Te around the g.s. and around 200 keV, respectively.

### B. Origin of new new positive-parity states in $^{137}$I

The appearance of the possible $(3/2^+)$ states is uniquely identified in this work (see Fig. 8). These states appear in the neighboring $^{135}$I, where the g.s. spin-parity is the same as in the other odd-$A$ I isotopes, including $A = 137$. These states cover several possibilities in $A = 135$ with log $ft$ around 7.4–7.5 and, together with the $11/2^+$ possibilities, up to 8.1 [12]. The candidates in $A = 137$, again similarly probable, are covered, except possibly $\Delta J = 2$ (of the g.s.) and also $\Delta J = 1$. Together with the spin-parity of $11/2^+$ they cover log $ft$ values from 6.8 to 7.7. For three of the observed states with $\Delta J = 2$ as the most probable scenario, also uniqueness can be assumed. For these first-forbidden transitions, this reflects the upper log $ft$ value as given in Table II.

The position of the $3/2^+$ states well matches the predicted excitation energy by the SM calculations. This can be seen in Fig. 9, where the direct correspondence and the predicted configuration as part of the $\nu f_{7/2}^2 \pi g_{7/2}^3$ multiplet may be traced. The competing $\pi d_{5/2}$ configuration is relevant only for states above 1.1 MeV and some of the higher-lying in energy experimental candidates. Nevertheless, they may correspond to a theoretical state with such origin (see color code). Some of the other propositions for these states such as $5/2^+$, $9/2^+$ (or $11/2^+$) also predicted nearby, would finally not be excluded.

Of the $11/2^+$ states, only those with the lowest $\nu f_{7/2}^2 \pi g_{7/2}^3$ configuration (see Table III) may be seen. Indeed, the lowest of these states among the experimental possibilities ($E_x = 620$ keV) has a remarkable theoretical ($E_x = 588$ keV) correspondence. The experimental possibilities for the second and third $11/2^+$ states, listed together with the first $13/2^+$

or fifth $3/2^+$ possibilities, respectively, have also perfect SM counterparts.

Concerning the $5/2^+$ states, we could classify with certitude the first excited states of them, based, as expected, on the predominant $\pi d_{5/2}$ configuration (see Table III with more than 40% probability). As it stays only at $E_x = 243$ keV, the orbital positioning may be inferred, and compared with other recent data with similar conclusions [4,7,23]. Moreover, this state is reported also in the heavier $^{139}$I at $E_x = 208$ keV. Compared to the same SM prediction ($E_x = 175$ keV) it has a rather good agreement [5,8]. Therefore, it can be concluded that no drastic change is present in these I isotopes for the $\pi d_{5/2}$ orbital. This behavior is different compared to the Sb isotopes [4,23]. Interestingly, in the $A = 135$ iodine neighbor, the second $5/2^+$ state is also observed in the vicinity of the first (e.g., at about 270 keV excitation energy difference) [12]. This is predicted also by the SM for $^{137}$I (see Fig. 9). We have observed another candidate within the excitation energy, e.g., the 373.1 keV state; however, it may also be assigned differently. The clear difference is based on the experimentally observed $I_\beta$ and respective log $ft$ values, which for the $5/2^+$ state in our work amount to 13.0 and 6.2, respectively. It is in a very good agreement with the data on both $5/2^+$ states in $^{135}$I, with respective values of 24.2/16.4 and 6.3/6.4. In $^{137}$I, two $5/2^+$ states with $d_{5/2}$ proton are predicted among the first six in about 1 MeV energy spacing. Thus, their distance appears larger than in the lighter neighbor. Indeed, two candidates can be traced among the excited states around 850 keV and 1.4 MeV (see Fig. 8).

The situation is similar with the $9/2^+$ states, two of which are based on the same proton excitation as the $5/2^+$ states, while the rest belong to the $\nu f_{7/2}^2 \pi g_{7/2}^3$ multiplet. It has to be underlined, however, that their wave functions are much more mixed than those of the $5/2^+$ states, with relative contributions of the order of 17%. Experimentally, only the first $9/2^+$ state is firmly assigned, while the other five candidates ($\Delta J = 1$ of the g.s.) are in competition with the possible $5/2^+$ assignment for three of the states. Alternatively, due to $\beta$ branching, also other possible $(3/2^+$ and $11/2^+)$ assignments can be considered for their most probable transition multipolarities. Based on the enhanced branch to the first $7/2^+$ state and the predicted second SM state, one may suggest that $9/2^+$ would be more likely for the 830 keV state than a spin-parity of $5/2^+$. For the higher-lying states, such a scenario may be relatively uncertain.

The most strongly fed $7/2^+$ states from the direct feeding of the $7/2^-$ g.s. state are naturally in good agreement with the $J = 7/2$ assignments. Any other different spin-parity would not present these strong branches, very visible in the level scheme (Fig. 8). This certainly excludes the $J = 5/2$ for the g.s. as, e.g., the feeding to the 243.6 and 713.5 keV states is clearly different. The log $ft$ values of the newly identified $(7/2^+)$ states are also of the order of 6. The first such state after the g.s. seems very likely positioned at 713.5 keV excitation energy, based on its experimental $I_\beta$ feeding, despite a slight underestimation in its theoretical energy (Fig. 9). Interestingly, in the earlier $\beta$ decay work, mostly the assigned as $7/2^+$ states are observed. The next such candidate, previously set but unassigned at 1169.0 keV

[12], is confirmed here at 1170.0 keV. In this work, we propose one additional candidate for $7/2^+$ at 1.4 MeV excitation energy (Fig. 9). These states are purely based on the proton $g_{7/2}^3$ configuration with the exception of the slightly competing $\pi g_{7/2}^2 d_{5/2}$ contribution for the $7/2_2^+$ state. Their theoretical correspondence is relatively good, as can be seen in Fig. 9.

As stated earlier, the nonobservation of states containing GT strength confirms that this channel is still blocked for $^{137}$I nucleus. The decay of $^{137}$Te is completely overtaken by the first-forbidden transitions from the dominating $\nu f_{7/2}^3 \pi g_{7/2}^2$ g.s. This is in full agreement with the SM calculations that also do not expect such branching at low energy. The first possible transition $7/2^-$ ($^{137}$Te) $\rightarrow$ $5/2^-$ ($^{137}$I) is expected at $E_x(5/2^-) = 3.8$ MeV with $B$(GT) of about 0.007, which is not found experimentally. It would be further interesting to investigate whether this strength can again be unblocked, e.g., due to the expectations of more mixing and an evolving collectivity also in the heavier neighbors.

## V. SUMMARY

In this work, we performed new $\beta$-decay spectroscopy of the $^{137}$Te nucleus to the daughter $^{137}$I. We observed several new transitions corresponding to first-forbidden branches to excited states in $^{137}$I. Due to the relatively weak $P_n$ ratio and insufficient statistics, the transitions after $\beta$-delayed neutron emission were strongly hindered and only a few indications of

states in $^{137}$I could be seen. Therefore, such an investigation would require more experimental data.

From the investigations performed in this work, it is interesting to highlight the nonobservation of GT strength for this $A = 137$ isotope, while a possible even-odd effect with the decrease of the GT strength at the expense of favored first-forbidden decay seems to be present. Furthermore, the strong effect of both $\pi g_{7/2}$ and $\pi d_{5/2}$ proton orbitals seems to completely dominate the structure of the $^{137}$I isotope observed in our data up to 2.4 MeV excitation energy.

The nucleus, being in a region of strong first-forbidden decays, has an interesting relation to studies of electron and antineutrino reactor spectral behavior [47,48]. The connection to the role of first-forbidden transitions, especially as forbidden decays cannot be neglected and need to be accounted for properly, is an active research domain with new experiments and methods [49,50]. Being an essential ingredient in understanding nuclear astrophysics mechanisms as well as reactor anti-neutrino spectra [49,51], these types of studies certainly merit deeper investigation.

[1] L. Coraggio, A. Covello, A. Gargano, N. Itaco, and T. Kuo, Prog. Part. Nucl. Phys. **62**, 135 (2009).

[2] B. A. Brown, Phys. Rev. Lett. **85**, 5296 (2000).

[3] J. Shergur, B. A. Brown, V. Fedoseyev, U. Köster, K.-L. Kratz, D. Seweryniak, W. B. Walters, A. Wöhr, D. Fedorov, M. Hannawald, M. Hjorth-Jensen, V. Mishin, B. Pfeiffer, J. J. Ressler, H. O. U. Fynbo, P. Hoff, H. Mach, T. Nilsson, K. Wilhelmsen-Rolander, H. Simon et al., Phys. Rev. C **65**, 034313 (2002).

[4] R. Lozeva, H. Naïdja, F. Nowacki, J. Dudek, A. Odahara, C.-B. Moon, S. Nishimura, P. Doornenbal, J.-M. Daugas, P.-A. Söderström, T. Sumikama, G. Lorusso, J. Wu, Z. Y. Xu, H. Baba, F. Browne, R. Daido, Y. Fang, T. Isobe, I. Kojouharov et al., Phys. Rev. C **93**, 014316 (2016).

[5] W. Urban, T. Rzaca-Urban, A. Korgul, J. L. Durell, M. J. Leddy, M. A. Jones, W. R. Phillips, A. G. Smith, B. J. Varley, I. Ahmad, L. R. Morss, and N. Schulz, Pays. Rev. C **65**, 024307 (2002).

[6] G. Häfner, R. Lozeva, H. Naïd ja, M. Lebois, N. Jovancevic, D. Thisse, D. Etasse, R. L. Canavan, M. Rudigier, J. N. Wilson, E. Adamska, P. Adsley, M. Babo, K. Belvedere, J. Benito, G. Benzoni, A. Blazhev, A. Boso, S. Bottoni, M. Bunce et al., Phys. Rev. C **103**, 034317 (2021).

[7] R. Lozeva, E. A. Stefanova, H. Naïdja, F. Nowacki, T. Rzaca-Urban, J. Wisniewski, W. Urban, I. Ahmad, A. Blanc, G. De France, F. Didierjean, G. Duchêne, H. Faust, J. P. Greene, U. Köster, P. Mutti, G. Simpson, A. G. Smith, T. Soldner, and C. A. Ur, Phys. Rev. C **98**, 024323 (2018).

[8] G. Häfner, R. Lozeva, H. Naïdja, M. Lebois, N. Jovancevic, D. Thisse, D. Etasse, R. L. Canavan, M. Rudigier, J. N. Wilson, E. Adamska, P. Adsley, A. Algora, M. Babo, K. Belvedere, J.

Benito, G. Benzoni, A. Blazhev, A. Boso, S. Bottoni et al., Phys. Rev. C **104**, 014316 (2021).

[9] V. Paar, Phys. Lett. B **39**, 466 (1972).

[10] G.V. Berghe, Z. Phys. **266**, 139 (1974).

[11] A. Korgul, W. Urban, T. Rzaca-Urban, M. Górska, J. L. Durell, M. J. Leddy, M. A. Jones, W. R. Phillips, A. G. Smith, B. J. Varley, M. Bentaleb, E. Lubkiewicz, N. Schulz, I. Ahmad, and L. R. Morss, Eur. Phys. J. A **12**, 129 (2001).

[12] M. Samri, G. J. Costa, G. Klotz, D. Magnac, R. Seltz, and J. P. Zirnheld, Z. Phys. A **321**, 255 (1985).

[13] E. Browne and J. K. Tuli, Nucl. Data Sheets **108**, 2173 (2007).

[14] B. Pfeiffer, J. P. Bocquet, A. Pinston, R. Roussille, M. Asghar, G. Bailleul, R. Decker, J. Greif, H. Schrader, G. Siegert et al., J. Phys. France **38**, 9 (1977).

[15] M. Asghar, J. P. Gautheron, G. Bailleul, J. P. Bocquet, J. Greif, H. Schrader, G. Siegert, C. Ristori, J. Crancon, and G. I. Crawford, Nucl. Phys. A **247**, 359 (1975).

[16] P. Armbruster, M. Asghar, J. P. Bocquet, R. Decker, H. Ewald, J. Greif, E. Moll, B. Pfeiffer, H. Schrader, F. Schussler, G. Siegert, and H. Wollnik, J. Phys. **139**, 213 (1976).

[17] U. Köster, H. Faust, T. Materna, and L. Mathieu, Nucl. Instrum. Methods Phys. Res., Sect. A **613**, 363 (2010).

[18] J. Kurpeta, W. Urban, T. Materna, H. Faust, U. Koster, J. Rissanen, T. Rzaca-Urban, C. Mazzocchi, A. G. Smith, J. F. Smith, J. P. Greene, and I. Ahmad (unpublished).

[19] G. Fioni, H. R. Faust, M. Gross, M. Hesse, P. Armbruster, F. Gönnenwein, and G. Münzenberg, Nucl. Instrum. Methods Phys. Res., Sect. A **332**, 175 (1993).

[20] L. Mathieu, O. Serot, T. Materna, A. Bail, U. Köster, H. Faust, O. Litaize, E. Dupont, C. Jouanne, A. Letourneau *et al.*, J. Instrum. **7**, P08029 (2012).

[21] M. Si, R. Lozeva, H. Naïdja, A. Blanc, J.-M. Daugas, F. Didierjean, G. Duchene, U. Köster, T. Kurtukian-Nieto, F. Le Blanc, P. Mutti, M. Ramdhane, and W. Urban, Phys. Rev. C (to be published).

[22] A. J. M. Plompen, O. Cabellos, C. De Saint Jean *et al.*, Eur. Phys. J. A **56**, 181 (2020).

[23] B. Moon, A. Jungclaus, H. Naïdja, A. Gargano, R. Lozeva, C.-B. Moon, A. Odahara, G. S. Simpson, S. Nishimura, F. Browne, P. Doornenbal, G. Gey, J. Keatings, G. Lorusso, Z. Patel, S. Rice, M. Si, L. Sinclair, P.-A. Söderström, T. Sumikama *et al.*, Phys. Rev. C **103**, 034320 (2021).

[24] J. Wu, S. Nishimura, P. Möller, M. R. Mumpower, R. Lozeva, C. B. Moon, A. Odahara, H. Baba, F. Browne, R. Daido, P. Doornenbal, Y. F. Fang, M. Haroon, T. Isobe, H. S. Jung, G. Lorusso, B. Moon, Z. Patel, S. Rice, H. Sakurai *et al.*, Phys. Rev. C **101**, 042801 (2020).

[25] M. Emeric and A. Sonzogni, Calculation program of log ft, web (accessed 2021), https://www.nndc.bnl.gov/logft/.

[26] M. Wang, W. J. Huang, F. G. Kondev, G. Audi, and S. Naimi, Chin. Phys. C **45**, 030003 (2021).

[27] J. Agramunt, J. L. Tain, M. B. Gómez-Hornillos, A. R. Garcia, F. Albiol, A. Algora, R. Caballero-Folch, F. Calviño, D. Cano-Ott, G. Cortés *et al.*, Nucl. Instrum. Methods Phys. Res., Sect. A **807**, 69 (2016).

[28] J. Liang, B. Singh, E. A. McCutchan, I. Dillmann, M. Birch, A. A. Sonzogni, X. Huang, M. Kang, J. Wang, G. Mukherjee *et al.*, Nucl. Data Sheets **168**, 1 (2020).

[29] H. Bateman, Proc. Cambridge Philos. Soc. **15**, 423 (1910).

[30] K. S. Krane, *Introductory Nuclear Physics* (John Wiley & Sons, New York, 1991).

[31] R. Thibes and S. L. Oliveira, Int. J. Pure Appl. Math. **93**, 879 (2014).

[32] T. Kibédi, T. W. Burrows, M. B. Trzhaskovskaya, P. M. Davidson, and C. W. Nestor Jr, Nucl. Instr. Meth. Phys. Res. A **589**, 202 (2008).

[33] W. Urban, A. Korgul, T. Rzaca-Urban, N. Schulz, M. Bentaleb, E. Lubkiewicz, J. L. Durell, M. J. Leddy, M. A. Jones, W. R. Phillips, A. G. Smith, B. J. Varley, I. Ahmad, and L. R. Morss, Phys. Rev. C **61**, 041301(R) (2000).

[34] S. Raman and N. B. Gove, Phys. Rev. C **7**, 1995 (1973).

[35] NNDC database (accessed 2021), https://www.nndc.bnl.gov.

[36] Yu. Khazov, A. Rodionov, and F. G. Kondev, Nucl. Data Sheets **112**, 855 (2011).

[37] W. Urban, W. Kurcewicz, A. Nowak, T. Razca-Urban, J. L. Durell, M. J. Leddy, M. A. Jones, W. R. Phillips, A. G. Smith, B. J. Varley, M. Bentaleb, E. Lubkiewciz, N. Schulz, J. Blomqvist, P. J. Daly, P. Bhattacharyya, C.T. Zhang, I. Ahmad, and L. R. Morss, Eur. Phys. J. A **5**, 239 (1999).

[38] F. Andreozzi, L. Coraggio, A. Covello, A. Gargano, T. T. S. Kuo, and A. Porrino, Phys. Rev. C **56**, R16 (1997).

[39] H. Naïdja, F. Nowacki, and B. Bounthong, Phys. Rev. C **96**, 034312 (2017).

[40] H. Naïdja and F. Nowacki, EPJ Web Conf. **193**, 01005 (2018).

[41] H. Naïdja, F. Nowacki, B. Bounthong, M. Czerwinski, T. Rzaca-Urban, T. Roginski, W. Urban, J. Wisniewski, K. Sieja, A. G. Smith, J. F. Smith, G. S. Simpson, I. Ahmad, and J. P. Greene, Phys. Rev. C **95**, 064303 (2017).

[42] E. Caurier, G. Martínez-Pinedo, F. Nowack, A. Poves, and A. P. Zuker, Rev. Mod. Phys. **77**, 427 (2005).

[43] B. Moon, C.-B. Moon, A. Odahara, R. Lozeva, P.-A. Söderström, F. Browne, C. Yuan, A. Yagi, B. Hong, H. S. Jung, P. Lee, C. S. Lee, S. Nishimura, P. Doornenbal, G. Lorusso, T. Sumikama, H. Watanabe, I. Kojouharov, T. Isobe, H. Baba *et al.*, Phys. Rev. C **96**, 014325 (2017).

[44] W.-T. Chou and E. K. Warburton, Phys. Rev. C **45**, 1720 (1992).

[45] S. H. Liu, J. H. Hamilton, A. V. Ramayya, A. Covello, A. Gargano, N. Itaco, Y. X. Luo, J. O. Rasmussen, J. K. Hwang, A. V. Daniel, G. M. Ter-Akopian, S. J. Zhu, and W. C. Ma, Phys. Rev. C **80**, 044314 (2009).

[46] W. Urban, W. R. Phillips, I. Ahmad, J. Rekawek, A. Korgul, T. Rzaca-Urban, J. L. Durell, M. J. Leddy, A. G. Smith, B. J. Varley, N. Schulz, and L. R. Morss, Pays. Rev. C **66**, 044302 (2002).

[47] L. Hayen, J. Kostensalo, N. Severijns, and J. Suhonen, Phys. Rev. C **99**, 031301(R) (2019).

[48] Th. A. Mueller, D. Lhuillier, M. Fallot, A. Letourneau, S. Cormon, M. Fechner, L. Giot, T. Lasserre, J. Martino, G. Mention, A. Porta, and F. Yermia, Phys. Rev. C **83**, 054615 (2011).

[49] M. Fallot, S. Cormon, M. Estienne, A. Algora, V. M. Bui, A. Cucoanes, M. Elnimr, L. Giot, D. Jordan, J. Martino, A. Onillon, A. Porta, G. Pronost, A. Remoto, J. L. Taín, F. Yermia, and A.-A. Zakari-Issoufou, Phys. Rev. Lett. **109**, 202504 (2012).

[50] L. Hayen, J. Kostensalo, N. Severijns, and J. Suhonen, Phys. Rev. C **100**, 054323 (2019).

[51] A. Algora, D. Jordan, J. L. Taín, B. Rubio, J. Agramunt, A. B. Perez-Cerdan, F. Molina, L. Caballero, E. Nácher, A. Krasznahorkay, M. D. Hunyadi, J. Gulyás, A. Vitéz, M. Csatlós, L. Csige, J. Äysto, H. Penttilä, I. D. Moore, T. Eronen, A. Jokinen *et al.*, Phys. Rev. Lett. **105**, 202501 (2010).